Available online at www.sciencedirect.com

ScienceDirect

Journal of Magnesium and Alloys 6 (2018) 375–383

www.elsevier.com/locate/jma

Full Length Article

Atomistic calculations of surface and interfacial energies of $Mg_{17}Al_{12}$–Mg system

F.X. Wang [a,b,*], B. Li [a,b]

[a] Department of Chemical and Materials Engineering, University of Nevada, Reno, NV 89557, USA
[b] Nevada Institute for Sustainability, University of Nevada, Reno, NV 89557, USA

Received 13 December 2017; accepted 14 August 2018
Available online 12 September 2018

Abstract

It is well known that precipitation hardening in magnesium (Mg) alloys is far less effective than in aluminum alloys. Thus, it is important to understand the surface and interfacial structure and energetics between precipitates and matrix. In upscale modeling of magnesium alloys, these energy data are of great significance. In this work, we calculated the surface and interfacial energies of $Mg_{17}Al_{12}$–Mg system by carefully selecting the surface or interface termination, using atomistic simulations. The results show that, the higher fraction of Mg atoms on the surface, the lower the surface energy of $Mg_{17}Al_{12}$. The interfacial energy of Mg/$Mg_{17}Al_{12}$ was calculated in which the Burgers orientation relationship (OR) was satisfied. It was found that the $(011)_P|(0002)_{Mg}$ interface has the lowest interfacial energy (248 mJ/m^2). Because the Burgers OR breaks when $\{10\bar{1}2\}$ twin occurs, which reorients the matrix, the interfacial energy for $Mg_{17}Al_{12}$ and a $\{10\bar{1}2\}$ twin was also calculated. The results show that after twinning, the lowest interfacial energy increases by 244 mJ/m^2, and the interface becomes highly incoherent due to the change in orientation relationship between $Mg_{17}Al_{12}$ and the matrix.

Keywords: $Mg_{17}Al_{12}$; Surface energy; Interfacial energy; Atomistic simulation.

1. Introduction

In recent years, magnesium (Mg) and its alloys have received significant attention due to their low densities and high specific strength. These properties make Mg alloys attractive for structural applications where improved fuel efficiency is needed [1–4]. Mg–Al alloys are the most common commercial Mg alloys, and have been used as model alloys for fundamental research on deformation mechanisms and mechanical behavior. The β-phase ($Mg_{17}Al_{12}$) is the primary equilibrium precipitates which act as strengthening phase for Mg alloys. Generally, $Mg_{17}Al_{12}$ precipitates increase the strength of Mg alloys by interacting with dislocation motion [5–7]. Discontinuous precipitation of $Mg_{17}Al_{12}$ may take place along high angle grain boundaries and grow into a cellular morphology [8,9]. In contrast, continuous precipitation occurs inside the matrix of individual grains by forming large plates parallel to the basal plane of the matrix [10]. Continuous precipitates follow the Burgers orientation relationship (OR) with respective to the matrix: $(0001)_{Mg}||(011)_P$, $[2\bar{1}\bar{1}0]_{Mg}||[1\bar{1}1]_P$ [8,11–14].

The effect of $Mg_{17}Al_{12}$ on mechanical behavior of Mg alloys has been studied by a number of researchers. Robson et al. [15] calculated the hardening effect based on Orowan's mechanism in terms of precipitate shape and habit plane. Their results suggested that the plate-like precipitates parallel to the basal plane are ineffective to impede basal slip; however, they may hinder twin growth, because precipitates inside a twin can provide a back-stress that prevents the plastic relaxation. This calculation was based on interaction between precipitates and "twinning dislocations" that can only glide on the $\{10\bar{1}2\}$ twinning plane. Such interaction was questioned by recent works that have suggested that $\{10\bar{1}2\}$ mode

* Corresponding author at: Department of Chemical and Materials Engineering, University of Nevada, Reno, NV 89557, USA.
E-mail address: fangxi.wang@nevada.unr.edu (F.X. Wang).

https://doi.org/10.1016/j.jma.2018.08.005

is not mediated by twinning dislocations but by atomic shuffling [16]. Li and Zhang showed that the twinning shear for $\{10\bar{1}2\}\langle 10\bar{1}\bar{1}\rangle$ mode should be zero [16]. Consequently, twin-precipitate interaction should be minimal, which explains why precipitate hardening in magnesium alloy is not as effective as alloys with cubic structures [6]. Liao et al. [17,18] simulated interactions between a $Mg_{17}Al_{12}$ precipitate and prismatic slip and basal slip in magnesium using atomistic simulations. Their results indicated that a basal dislocation is able to bypass the precipitate without creating a dislocation loop around the precipitate, suggesting a rather weak interaction. In contrast, a prismatic dislocation may cut through the precipitate. They also showed that the interface between the precipitate and the matrix is incoherent and the interfacial strength is weak. $Mg/Mg_{17}Al_{12}$ interfaces can act as a source of crack initiation to influence the fracture behavior [19]. $Mg/Mg_{17}Al_{12}$ interface also significantly influences the corrosion behavior [20,21] of Mg alloys because the free corrosion potential of $Mg_{17}Al_{12}$ phase is relatively more positive in a NaCl solution.

According to phase field simulation results by Han et al. [22–24], the competition between interfacial energy and elastic strain energy determines the morphology of $Mg_{17}Al_{12}$ phase [7]. In their simulation, anisotropic interfacial energy and interface mobility, and elastic strain energy incorporated in their phase field model, but how the energy data was obtained was not available. Hutchinson et al. [14] calculated the $Mg/Mg_{17}Al_{12}$ interfacial energies, but the effect of surface termination of $Mg_{17}Al_{12}$ was not considered. Xiao et al. [25] calculated the surface energies of $Mg_{17}Al_{12}$ but surface termination was not considered as well.

In this work, we performed atomistic simulations to calculate the surface and interfacial energies of $Mg/Mg_{17}Al_{12}$ system. Surface termination and interfacial structure were taken into consideration. Such data are of importance for further understanding the mechanical properties of Mg alloys and for upscale simulation and modeling.

2. Simulation method

We used XMD molecular dynamics (MD) simulation package to perform our calculations. The embedded atom method (EAM) [26,27] interatomic potential for Mg and Al developed by Liu et al. [28] was used. This potential has been used in extensive MD simulations of mechanical properties for Mg and Mg alloys [29–31]. More recently, Wu and Curtin [32] developed a modified EAM (MEAM [33]) potential for Mg, in which the stacking fault energy has a better accuracy. Ovito [34] was used for graphic visualization.

The method for our calculations is schematically shown in Fig. 1 [35]. First, we constructed a $Mg_{17}Al_{12}$ crystal which has a complex structure. They system contains a total of 928,000 atoms. The dimension of the system was 42(X) × 42(Y) × 11(Z) nm. The X, Y and Z are along the [100], [010] and [001] directions, respectively. The temperature in the simulation was kept constant at 10 K. Free surface conditions was applied to all three dimensions. The system was relaxed for 30 ps to minimize the potential energy of the system. To calculate the surface energy, first, we select atoms inside Box A which is in the center of the system and away from the free surfaces. The average potential energy of Al and Mg atoms were calculated. These energies were used as the baseline energy for calculating the surface energy. Because the system is sufficiently large, the effect of free surfaces on the baseline energy can be neglected. Second, we selected another Box B which contains a portion of the free surface of interest [35], and the average potential energy of Al and Mg atoms inside Box B were calculated. Then the surface energy γ_{sur} can be calculated as:

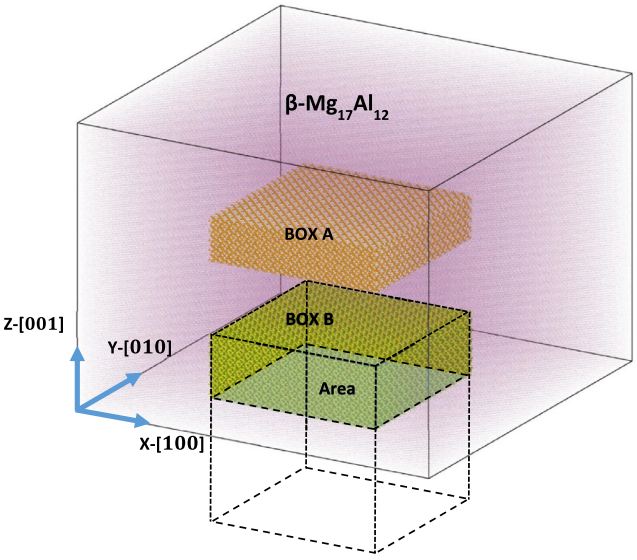

Fig. 1. Schematic of calculation method for surface energies of $Mg_{17}Al_{12}$ [35]. A $Mg_{17}Al_{12}$ precipitate was constructed. Atoms inside Box A are used for calculating the baseline energy of Al and Mg atoms, and Box B for calculating the surface energies.

$$\gamma_{sur} = \frac{(E'_{Mg} - E_{Mg}) \times N_{Mg} + (E'_{Al} - E_{Al}) \times N_{Al}}{A} \quad (1)$$

where E_{Mg} and E_{Al} are the average potential energies per atom for Mg and Al from box A; E'_{Mg} and E'_{Al} are the average potential energies per atom for Mg and Al from box B; N_{Mg} and N_{Al} are the number of Mg and Al atoms in box B; A is the area of the free surface that is contained in Box B (in the case of Fig. 1, the area is on the bottom XY-surface in box B).

The calculation of the surface energies of $Mg_{17}Al_{12}$ is complicated by the fact that there are many possible surface terminations or configurations. This complication is shown in Fig. 2. Thus, all the possible surface terminations should be considered in the calculation. We calculated each surface energy of different terminations by removing the outermost atoms of each surface plane layer by layer to find the lowest surface energy termination. The highest surface energy termination was obtained as well. Fig. 2(a) shows the (010) surface structure with the viewing direction being [010]. It can be observed that the structure presents repeating units in all three dimensions, as indicated by the yellow arrows, and this simplifies our calculations. For instance, along the Z-[001],

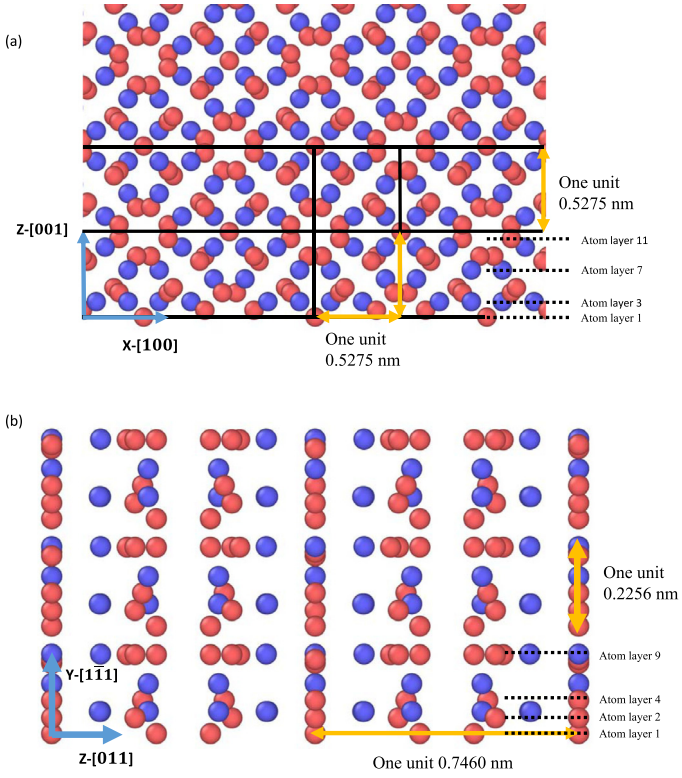

Fig. 2. Possible surface terminations for $Mg_{17}Al_{12}$ [35]. Mg atoms are in red and Al atoms in blue. (a) The (010) surface configuration of the simulation system for $Mg_{17}Al_{12}$. (b) The structure of $Mg_{17}Al_{12}$ along the [21$\bar{1}$], [1$\bar{1}$1] and [011] directions.

the structure repeats itself every unit length as indicated by the yellow arrow. Similar repetition can be seen along the X-[100] direction.

In the Burgers OR, i.e., $(0001)_{Mg}||(011)_P$, $[2\bar{1}\bar{1}0]_{Mg}||[1\bar{1}1]_P$, the surfaces of $Mg_{17}Al_{12}$ are normal to the [011], [1$\bar{1}$1] and [21$\bar{1}$], thus, the energies of these surfaces also need to be calculated. The system was reoriented to obey a Burgers OR precipitate, and the surface energies termination was determined using the above method [35]. Fig. 2(b) shows the structure of $Mg_{17}Al_{12}$ when the viewing direction is reoriented to the [21$\bar{1}$]. Similarly, the repeating units along each direction can be observed.

To calculate the energies of Mg/$Mg_{17}Al_{12}$ interfaces that satisfies the Burgers OR, we constructed a big system with dimensions of 29 × 29 × 56 nm (~2.25 million atoms). The system contains both the Mg matrix and the $Mg_{17}Al_{12}$ precipitate, as shown in Fig. 3. The temperature condition and the surface condition were same as in the surface energy calculation. They system was relaxed for 6 ps. Atoms inside Box A which is inside the Mg matrix were selected to calculate the baseline energy of the Mg atoms of the matrix. Atoms inside Box B were selected to calculate the baseline energy of Al atoms and Mg atoms of the $Mg_{17}Al_{12}$. Another Box C which comprises the Mg/$Mg_{17}Al_{12}$ interface was selected to calculate the interfacial energy. The interfacial energy γ_{int} can be calculated as:

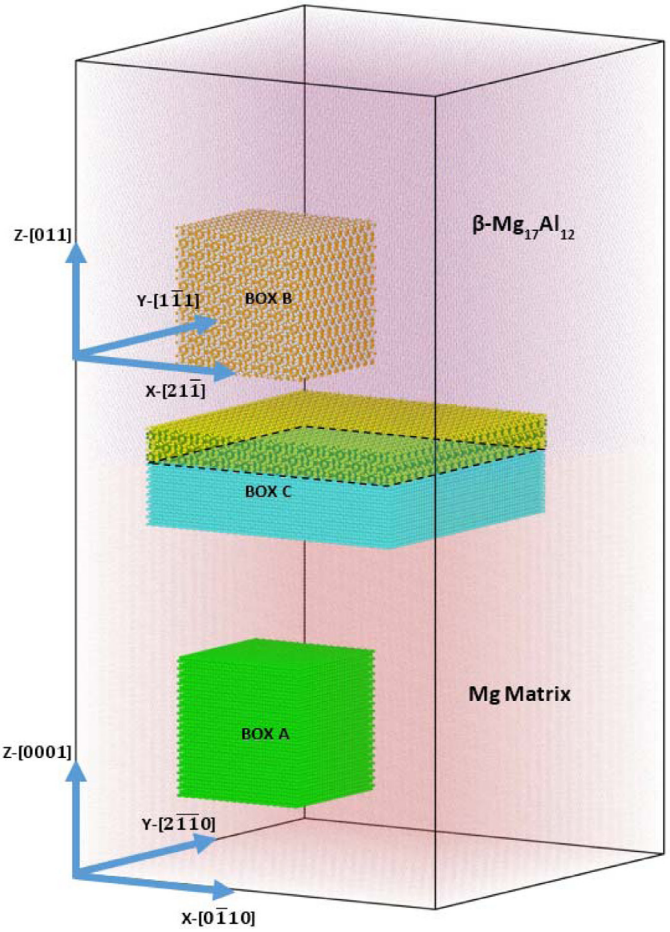

Fig. 3. The method for calculating the Mg/$Mg_{17}Al_{12}$ interfacial energy [35]. Box A and B were used for calculating the baseline energies of atoms in Mg matrix and $Mg_{17}Al_{12}$. Box C was used for calculating the interfacial energy.

$$\gamma_{int} = \frac{(E'_{Mg(m)} - E_{Mg(m)}) \times N_{Mg(im)} + (E'_{Mg(p)} - E_{Mg(p)}) \times N_{Mg(ip)} + (E'_{Al(p)} - E_{Al(p)}) \times N_{Al(ip)}}{A} \quad (2)$$

where $E_{Mg(p)}$ and $E_{Al(p)}$ are the average potential energies per atom for Mg and Al in Box A; $E_{Mg(m)}$ is the average potential energy per atom for Mg in Box B; $E'_{Mg(p)}$ and $E'_{Al(p)}$ are the average potential energies per atom for Mg and Al in the precipitate in Box C; $E'_{Mg(m)}$ is the average potential energy per atom for Mg in the matrix in Box C; $N_{Mg(ip)}$ and $N_{Al(ip)}$ are the number of Mg and Al atoms in the precipitate in box C; $N_{Mg(im)}$ is the number of Mg from the matrix in box C; A is the area of the Mg/$Mg_{17}Al_{12}$ interface contained in Box C [35].

After $\{10\bar{1}2\}\langle 10\bar{1}\bar{1}\rangle$ twinning, the matrix was reoriented by 90° around the $[2\bar{1}\bar{1}0]$ zone axis. The Mg_{twin}/$Mg_{17}Al_{12}$ interfacial energy was then calculated.

3. Results

As shown in Fig. 2(a), the $Mg_{17}Al_{12}$ β-phase presents repeating structural unit in all three dimensions. For the viewing direction of [010] in Fig. 2(a), each structural unit contains

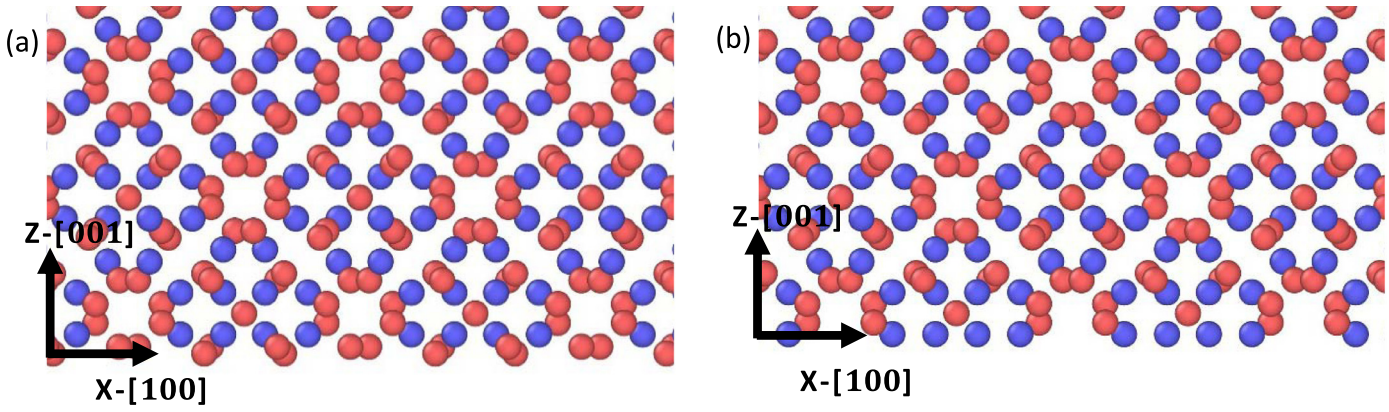

Fig. 4. (a) The (001) surface structure of $Mg_{17}Al_{12}$ with the lowest surface energy. The viewing direction is along [010]. (b) The (001) surface structure with the highest surface energy [35].

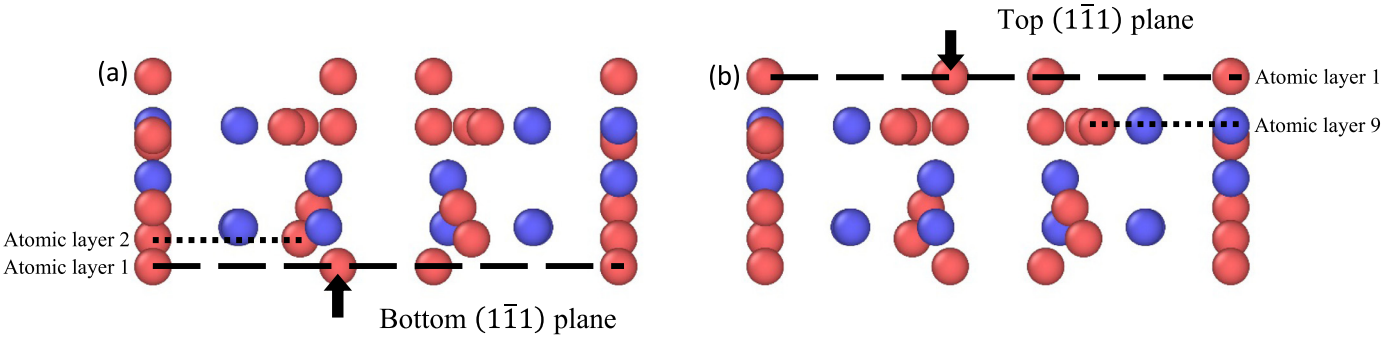

Fig. 5. The same surface layer may have different surface energies due to the different atomic layers underneath the surface layer. When atomic layer 1 becomes the surface, it may have either atomic layer 2 (a) or atomic layer 9 (b) as the underlying layer, which will give different surface energies.

twelve (001) planes or atomic layers. Therefore, we calculated the surface energies for all the twelve different surface terminations for (010). The results show that, when the 8th atomic layer was exposed as the surface termination, the surface energy is the lowest which equals 742.7 mJ/m^2. The highest surface energy appears when the 10th atomic layer was exposed as the surface termination, and has a value of 980 mJ/m^2. The structures with the lowest and the highest surface energy are shown in Fig. 4(a) and (b), respectively.

As shown in Fig. 2(a), the low index configuration along the [100], [010] and [001] directions present centrosymmetry that simplifies our calculation of the surface energy. However, this is not the case for the [21$\bar{1}$], [1$\bar{1}$1] and [011] directions. The structure in the new orientation also shows repeating units along each direction, but only along the [011] direction the structure has centrosymmetry. Additionally, for different directions, the number of atomic layers in the repeating unit varies. The lack of centrosymmetry is demonstrated in Fig. 5(a) and (b). Along the viewing direction of [21$\bar{1}$], although the bottom (1$\bar{1}$1) and the top (1$\bar{1}$1) surface have exactly the same atomic structure, the underlying atomic layers are very different. For example, the structures of layer 2 in Fig. 5(a) and layer 9 in Fig. 5(b) differ significantly. Therefore, although the (1$\bar{1}$1) surface layers in Fig. 5(a) and (b) have the same atomic structure, the surface energy is expected to differ. When atomic layer 1 was exposed as the bottom (1$\bar{1}$1) surface (Fig. 5(a)), this termination gives a surface energy of 829 mJ/m^2. In contrast, when atomic layer 1 was exposed as the top (1$\bar{1}$1) surface (Fig. 5(b)), this termination gives a surface energy of 820 mJ/m^2. Our results show that due to the difference in underlying atoms, the surface energy may change by as much as 150 mJ/m^2 for a specific surface layer.

Table 1
Surface energies for $Mg_{17}Al_{12}$ [35].

Plane	Direction of layer removal	Lowest (mJ/m^2)	Highest (mJ/m^2)
(001)	[001]	743	980
(21$\bar{1}$)	[21$\bar{1}$]	789	1053
(2$\bar{1}$1)	[$\bar{2}$1$\bar{1}$]	763	953
(1$\bar{1}$1)	[1$\bar{1}$1]	776	960
(1$\bar{1}$1)	[$\bar{1}$1$\bar{1}$]	761	898
(011)	[011]	716	1009

By incorporating all the possible surface configurations, we calculated the surface energies and the results are summarized in Table 1. In terms of (1$\bar{1}$1) bottom surface, the lowest surface energy appears when the 6th atomic layer becomes the bottom surface (776 mJ/m^2 as in Fig. 6(a)). When the 9th atomic layer becomes the bottom surface, the surface energy is the highest (960 mJ/m^2 as in Fig. 6(b)). In terms of (1$\bar{1}$1) top surface, when the 2nd atomic layer becomes the top

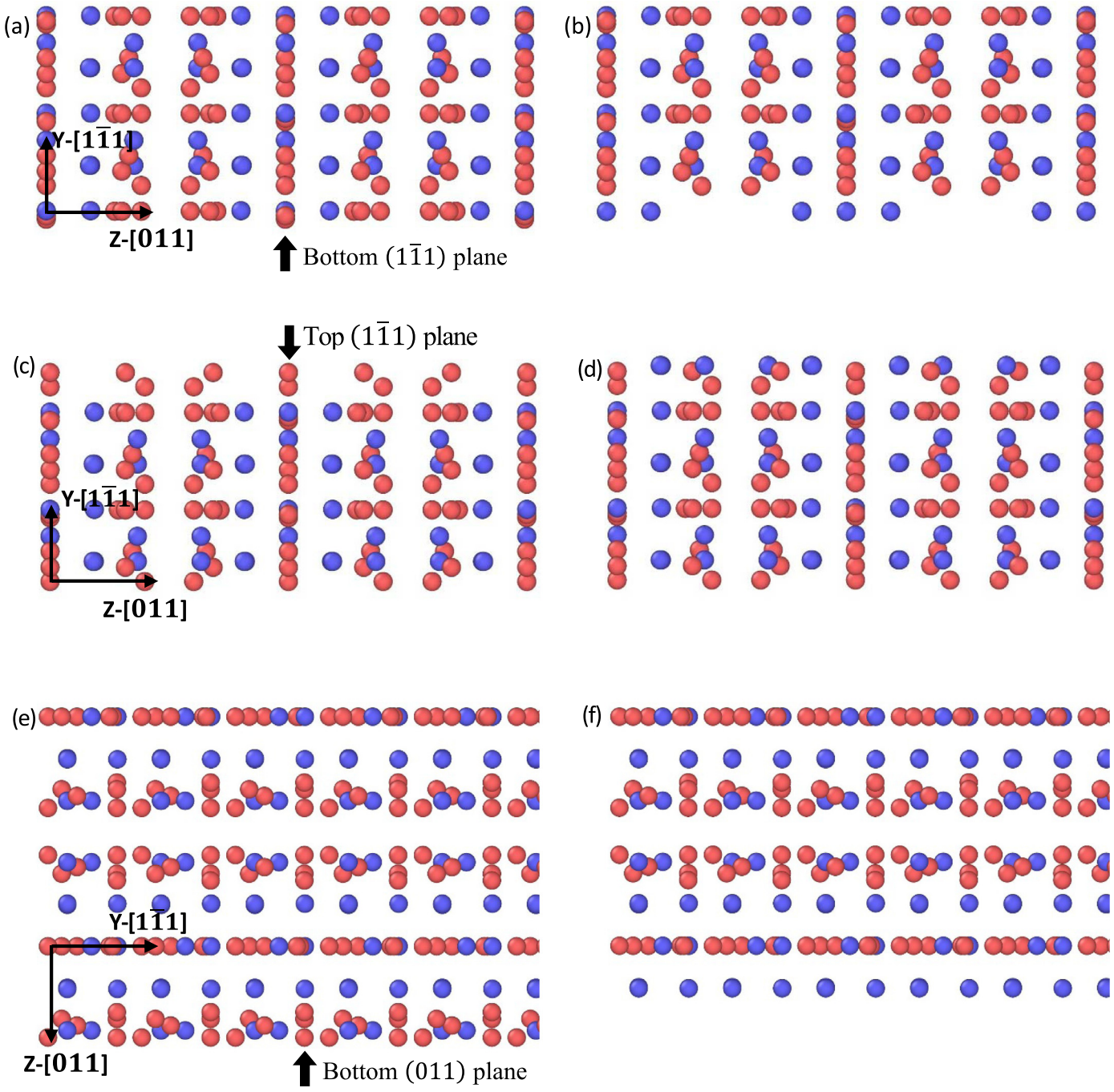

Fig. 6. (a) Bottom (1$\bar{1}$1) surface that has the lowest surface energy. (b) Bottom (1$\bar{1}$1) surface that has the highest surface energy. (c) Top (1$\bar{1}$1) surface that has the lowest surface energy. (d) Top (1$\bar{1}$1) surface that has the highest surface energy. [35] (e) Bottom (011) surface that has the lowest surface energy. (f) Bottom (011) surface that has the highest surface energy.

surface, the surface energy has the lowest value (761 mJ/m^2 as in Fig. 6(c)). When the 3rd atomic layer becomes the top surface, the surface energy is the highest (898 mJ/m^2 as in Fig. 6(d)).

For (011) surface, only the energies from removing atomic layer in one direction is shown because of the symmetry. Fig. 6(e) shows the (011) bottom surface that has the lowest surface energy (716 mJ/m^2), and Fig. 6(f) shows the (011) bottom surface which has the highest surface energy (1009 mJ/m^2).

The interfacial energies were calculated based on the Burgers OR. The effect of (1$\bar{1}$1) surface termination of $Mg_{17}Al_{12}$ on the interfacial energy was examined and the results are summarized in Table 2, which shows the interfacial energies when different atomic layers become the free surface layer (both top and bottom) of the precipitate. We also calculated the interfacial energies of different (1$\bar{1}$1) terminations after

Table 2
Effect of $(1\bar{1}1)$ surface termination on the Interfacial energy.

Bottom, $[1\bar{1}1]$			Top, [111]		
Number of atomic layer	Matrix	Twin	Number of atomic layer	Matrix	Twin
6	449	425	2	441	462
7	447	421	1	443	451
8	426	409	9	445	438
9	407	424	8	423	427
1	444	453	7	426	446
2	430	423	6	428	439
3	424	418	5	426	429
4	454	459	4	444	436
5	440	440	3	433	417

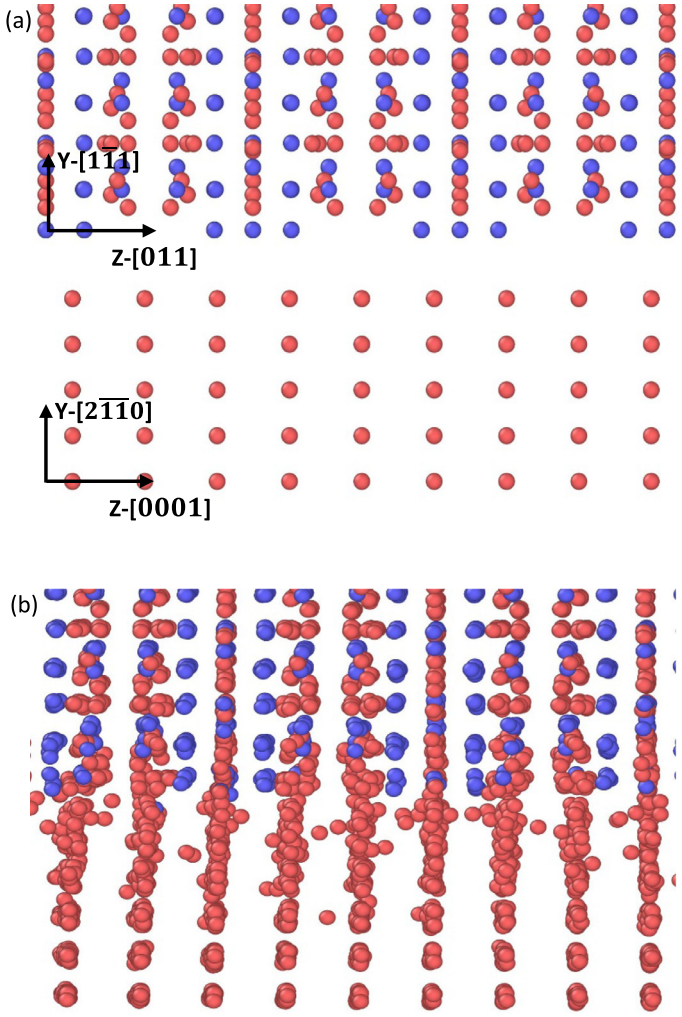

Fig. 7. (a) The initial structure before relaxation when a $(1\bar{1}1)$ surface of the $Mg_{17}Al_{12}$ was bonded to a $(2\bar{1}\bar{1}0)$ plane of the Mg matrix. (b) The interfacial structure after relaxation, which is rather incoherent.

$\{10\bar{1}2\}\langle 10\bar{1}\bar{1}\rangle$ twinning which reorients the Mg matrix, and the results are shown in Table 2 as well. Fig. 7(a) shows one of the initial interface configurations (i.e., before relaxation) in which a $(1\bar{1}1)$ plane of the $Mg_{17}Al_{12}$ was bonded to a $(2\bar{1}\bar{1}0)$ plane of the Mg matrix. After relaxation, the two phases bonded together, and the interface becomes rather incoherent, as shown in Fig. 7(b).

Table 3
Interfacial energies for $Mg/Mg_{17}Al_{12}$ and $Mg_{twin}/Mg_{17}Al_{12}$.

	Type of interface	Interfacial energy (mJ/m^2)
$Mg/Mg_{17}Al_{12}$	$(2\bar{1}\bar{1})_P\|(0\bar{1}10)_{Mg}$	390
	$(\bar{2}\bar{1}1)_P\|(0\bar{1}10)_{Mg}$	400
	$(1\bar{1}1)_P\|(2\bar{1}\bar{1}0)_{Mg}$	449
	$(\bar{1}1\bar{1})_P\|(2\bar{1}\bar{1}0)_{Mg}$	440
	$(011)_P\|(0002)_{Mg}$	248
$Mg_{twin}/Mg_{17}Al_{12}$	$(2\bar{1}\bar{1})_P\|(0002)_{Mg}$	397
	$(\bar{2}\bar{1}1)_P\|(0002)_{Mg}$	352
	$(1\bar{1}1)_P\|(2\bar{1}\bar{1}0)_{Mg}$	424
	$(\bar{1}1\bar{1})_P\|(2\bar{1}\bar{1}0)_{Mg}$	462
	$(011)_P\|(0\bar{1}10)_{Mg}$	492

From the results in Table 2, it can be observed that the change in surface termination of $Mg_{17}Al_{12}$ does not alter the interfacial energy significantly. Thus, the interfacial energy is relatively insensitive to surface termination of the precipitate. Therefore, for other interfaces, to reduce the amount of calculation, we used the lowest and highest surface energy terminations of the $Mg_{17}Al_{12}$ to calculate the interfacial energies. So, except for $(011)_P|(0002)_{Mg}$ interface, each interface has two data points. The results are shown in Table 3. Fig. 8(a) shows the initial structure (i.e., before relaxation) when a (011) plane of the $Mg_{17}Al_{12}$ was bonded to a (0002) plane of the Mg matrix. After relaxation (Fig. 8(b)), it can be seen that the interface retains a good registry with minimal distortion to the lattice at the vicinity of the interface.

After $\{10\bar{1}2\}\langle 10\bar{1}\bar{1}\rangle$ twinning, the interface in Fig. 8 is altered by twinning. The original $(011)_P|(0002)_{Mg}$ interface is now changed to $(011)_P|(0\bar{1}10)_{Mg}$ interface, as shown in Fig. 9(a), which is the initial structure before relaxation. After relaxation, as shown in Fig. 9(b), the relaxed interface structure is rather disordered, indicating that the interface structure is highly incoherent.

4. Analysis and discussion

4.1. Surface energy of $Mg_{17}Al_{12}$

From the surface energies shown in Table 1, it can be seen that the lowest surface energy termination appears in the (011) surface which gives a value of 716 mJ/m^2. This is likely due to the complex body-centered-cubic (BCC) structure of $Mg_{17}Al_{12}$ in which the (011) plane is the closed packed plane and gives the low surface energy [36]. Xiao et al. [25] showed in their work that the (110) surface energy of $Mg_{17}Al_{12}$ β-phase is 716 mJ/m^2. Thus, the agreement is very good. Additionally, Xiao et al. [25] also reported surface energies of (100) plane (806 mJ/m^2) and (111) plane (790 mJ/m^2) of the β-phase. It can be seen that these values fall in the range of our calculations (743–980 mJ/m^2 for (100) and 776–960 mJ/m^2 for (111)). Because no details of surface termination was provided in [25], discrepancies can be expected. Ning et al. [37] performed density functional

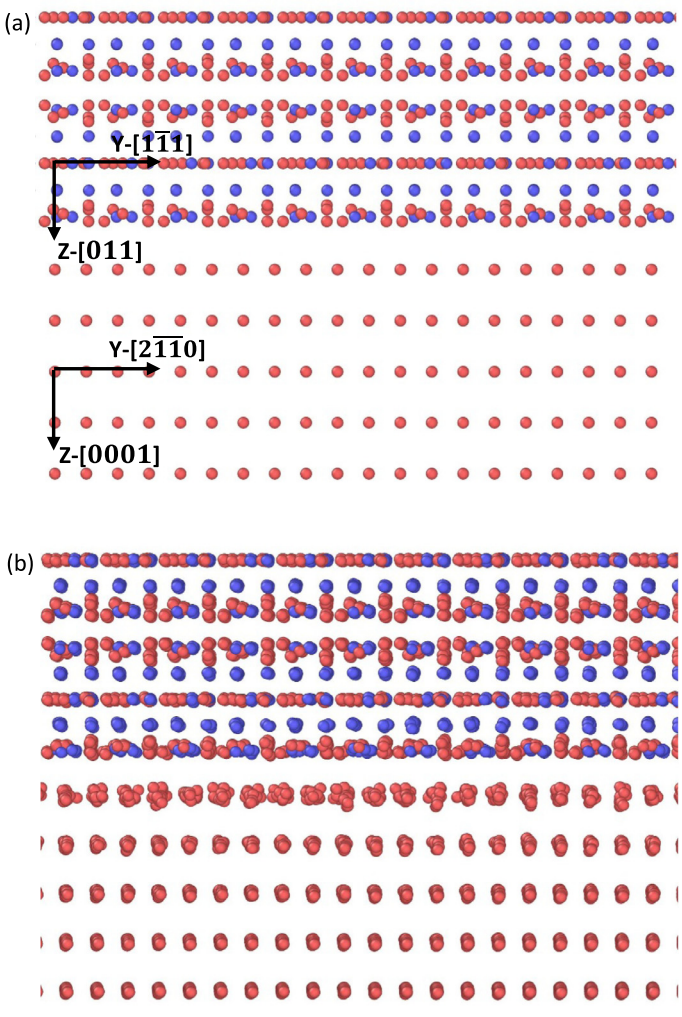

Fig. 8. (a) The initial structure before relaxation when a (011) surface of the $Mg_{17}Al_{12}$ was bonded to a (0002) basal plane of the Mg matrix. (b) The interfacial structure after relaxation, which retains a good registry and minimal lattice distortion.

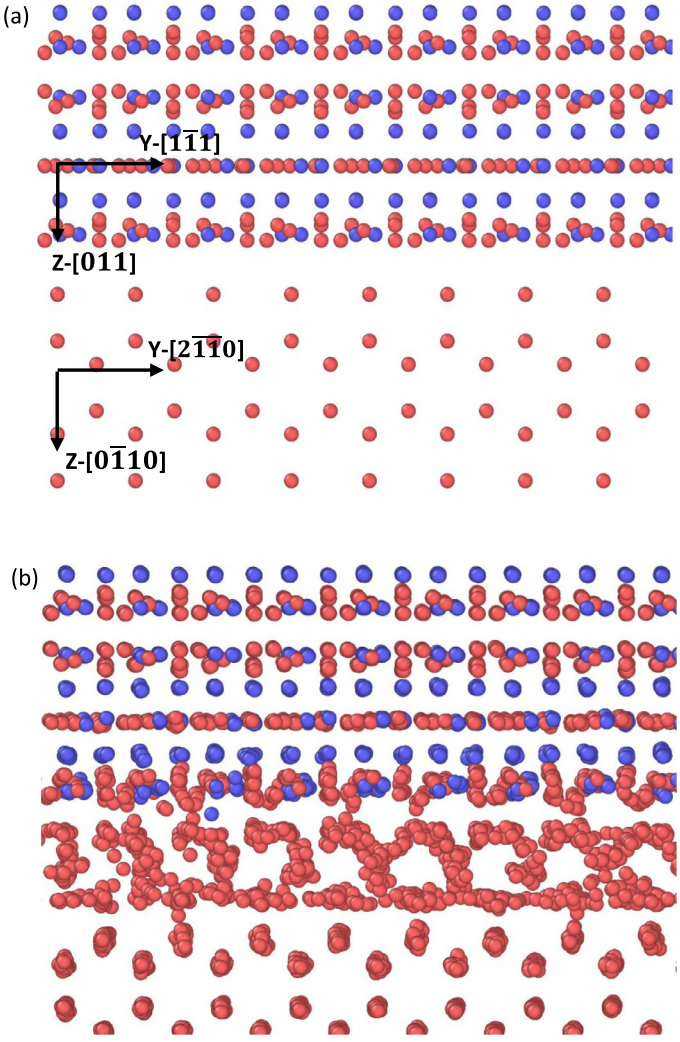

Fig. 9. Because $\{10\bar{1}2\}\langle 10\bar{1}\bar{1}\rangle$ reorients the Mg matrix, after twinning, the original $(011)_P|(0002)_{Mg}$ interface in Fig. 8 now becomes $(011)_P|(0\bar{1}10)_{Mg}$ interface. (a) Before relaxation. (b) After relaxation. The interfacial structure and energy significantly change.

theory (DFT) calculation for the surface energy of (001) plane of $Mg_{17}Al_{12}$, and the value is 799 mJ/m^2. From the (001) surface structure used for the surface energy calculations in [25,37], we can see that the surface termination in these calculations is identical to our case in which the atomic layer 1 is the surface (Fig. 2(a)), and our result is 783 mJ/m^2. Again, the agreement is satisfactory.

Our results in Table 2 also show that, when centrosymmetry is absent, the surface energy also relies on the subsurface atoms next to the surface atoms. For example, for the (1$\bar{1}$1) surface of $Mg_{17}Al_{12}$, the thickness of the atomic layers 6–9 is about 0.026 nm (Fig. 2(b)). These atoms can be considered as on the same surface that has the highest atomic density. This surface termination gives lowest surface energy for the bottom (1$\bar{1}$1) plane (Fig. 6(a)). However, when these atoms become the top (1$\bar{1}$1) surface, the surface energy is not the lowest due to the different subsurface atomic layers. Actually, the surface with the lowest energy is when the atomic layer 2 becomes the top (1$\bar{1}$1) surface (Fig. 6(c)).

Furthermore, Figs. 4(b) and 6(b), (d), and (f) show that the high surface energy terminations contain more Al atoms. This can be understood from the difference in potential energy of Al atoms (~0.0274 eV/atom) and Mg atoms (~0.0198 eV/atom). Therefore, the number of Al atoms becomes a more significant factor contributing to the surface energy. In contrast, surfaces with a higher fraction of magnesium atoms generate lower surface energies.

4.2. Interfacial energy of $Mg/Mg_{17}Al_{12}$

The interfacial energies for $Mg/Mg_{17}Al_{12}$ in Table 3 clearly show that, in the Burgers OR, $(011)_P|(0002)_{Mg}$ type of interfaces gives the lowest interfacial energy (248 mJ/m^2). In the work by Han et al. [38], the estimated interfacial energy value falls in the range of 140–390 mJ/m^2. In the thermodynamics calculations by Hutchinson et al. [14], the interfacial energy was shown as 430 mJ/m^2, which is close to the

values of other types of interfaces, e.g., $(21\bar{1})_P|(0\bar{1}10)_{Mg}$ and $(1\bar{1}1)_P|(2\bar{1}\bar{1}0)_{Mg}$. Thus, our calculation result is reasonable. Li et al. [39] reported an energy value of 100 mJ/m^2 for incoherent interfaces. This value appears to be rather low and how this value was obtained was not provided. As shown in Fig. 8, after relaxation, the $(011)_P|(0002)_{Mg}$ interface has a good registry and lattice distortion near the interface is much less severe if compared to other types of interfaces. Because the interfacial energy and the elastic strain between a precipitate and a matrix largely determine the morphology of the precipitates [7], accordingly the $(011)_P|(0002)_{Mg}$ interface is energetically more favorable. This well explains why equilibrium $Mg_{17}Al_{12}$ precipitates in Mg–Al alloys generally assume a plate-like morphology with the plate plane parallel to the basal plane of the Mg matrix.

From our results (Tables 2 and 3), it is noticeable that the interfacial energies do not change dramatically when $Mg_{17}Al_{12}$ surface termination changes and after twinning reorients the Mg matrix. However, for the $(011)_P|(0002)_{Mg}$ interface that has the lowest interfacial energy, twinning significantly changes the interfacial structure and the interfacial energy, as shown in Figs. 8 and 9. After twinning, the interfacial energy for this particular interface increases by 244 mJ/m^2. Interfacial energy of phase boundaries and grain boundaries is predominantly determined by the interaction of atoms that are located at the interface. Thus, the structure of the interface strongly influences the interfacial energy. In general, the more coherent of an interface, the lower the interfacial energy. For instance, coherent twin boundaries always have low interfacial energies (with one exception of $\{11\bar{2}1\}$ twin boundary in hexagonal close-packed metals in which a coherent twin boundary has a much higher energy than an incoherent twin boundary because of the strong repulsive atomic interaction in a coherent twin boundary due to the small interplanar spacing [40]). Thus, the interfacial energy is a measure of coherency of an interface. The significant increase in interfacial energy of $(011)_P|(0002)_{Mg}$ interface after twinning may have important implications for the mechanical properties of Mg–Al alloys.

It is well known that precipitate strengthening effect in Mg–Al alloys is much less than that in Al alloys. This has been attributed to geometry factors of $Mg_{17}Al_{12}$ phase [5,9]. When the $Mg_{17}Al_{12}$ precipitates assume plate-like morphology parallel to the basal plane, the effect of hindering basal slip, which is the easiest slip system in Mg alloys, is limited. Large spacing between the plates also reduces the strengthening effect. Efforts have been made [6,9] to modify the orientation of precipitates such that they are inclined or perpendicular to the basal plane. The improvement in strengthening is still insignificant. Thus, the Mg/$Mg_{17}Al_{12}$ interfacial structure and energetics need to be considered as well. Liao et al. [18] showed in their simulations that when a basal dislocation glides in contact with a $Mg_{17}Al_{12}$ precipitate, no dislocation loop was generated. Instead, the interface acts as a dislocation sink, likely due to the highly incoherent interface structure and the relatively high interfacial energy.

In fact, after $\{10\bar{1}2\}\langle 10\bar{1}\bar{1}\rangle$ twinning, the $Mg_{17}Al_{12}$ plates that are originally parallel to the basal plane become perpendicular to the basal plane. However, as seen in Fig. 9, after twinning, the original, low energy $(011)_P|(0002)_{Mg}$ interface becomes a more disordered, incoherent $(011)_P|(01\bar{1}0)_{Mg}$ with a much higher interfacial energy. This type of interfaces may reduce the strengthening effect in terms of dislocation-precipitate interaction. Thus, to design precipitate strengthened Mg alloys, interfacial structure and energy between the precipitates and the matrix should be considered as well.

5. Conclusion

In this work, we conducted atomistic calculations of surface and interfacial energies of Mg/$Mg_{17}Al_{12}$ system, by taking into account the effect of $Mg_{17}Al_{12}$ surface termination. The following conclusions can be reached:

(1) The surface energy of $Mg_{17}Al_{12}$ is sensitive to the surface termination. Generally, surfaces with higher fraction of magnesium atoms generate lower surface energies.
(2) The Mg/$Mg_{17}Al_{12}$ interfacial energy is relatively insensitive to the surface termination of $Mg_{17}Al_{12}$. $(011)_P|(0002)_{Mg}$ interface generates the lowest interfacial energy, and the interfacial structure has a good registry and minimal lattice distortion near the interface. This explains why equilibrium $Mg_{17}Al_{12}$ phase prefers a plate-like morphology parallel to the basal plane.
(3) After twinning, the original Burgers OR breaks and the interfacial structure and energies change. The original $(011)_P|(0002)_{Mg}$ interface that has the lowest interfacial energy now becomes $(011)_P|(01\bar{1}0)_{Mg}$ interface with a more incoherent structure and the interfacial energy increases by 244 mJ/m^2. Such a change in interfacial structure and energy may have important implications on the mechanical behavior of Mg–Al alloys.

Acknowledgments

Bin Li gratefully thank support from the U.S. National Science Foundation (CMMI-1635088).

References

[1] J. Hirsch, T. Al-Samman, Acta Mater. 61 (2013) 818–843, doi:10.1016/j.actamat.2012.10.044.
[2] B.L. Mordike, T. Ebert, Mater. Sci. Eng. A. 302 (2001) 37–45.
[3] B. Smola, I. Stulíková, F. von Buch, B.L. Mordike, Mater. Sci. Eng. A 324 (2002) 113–117, doi:10.1016/S0921-5093(01)01291-6.
[4] C. Frank, Magnesium Alloys-Design, Processing and Properties, Intech, India, 2011.
[5] J.B. Clark, Acta Metall. 16 (1968) 141–152, doi:10.1016/0001-6160(68)90109-0.
[6] J.-F. Nie, Metall. Mater. Trans. A 43 (2012) 3891–3939, doi:10.1007/s11661-012-1217-2.
[7] H. Liu, J.F. Nie, Mater. Sci. Technol. 0 (2017) 1–14, doi:10.1080/02670836.2017.1375749.
[8] S. Celotto, Acta Mater. 48 (2000) 1775–1787, doi:10.1016/S1359-6454(00)00004-5.

[9] J.F. Nie, Scr. Mater. 48 (2003) 1009–1015, doi:10.1016/S1359-6462(02)00497-9.
[10] D. Duly, J.P. Simon, Y. Brechet, Acta Metall. Mater. 43 (1995) 101–106, doi:10.1016/0956-7151(95)90266-X.
[11] A.F. Crawley, K.S. Milliken, Acta Metall. 22 (1974) 557–562. doi:10.1016/0001-6160(74)90152-7.
[12] M. Zhang, F. Ye, W.-Z. Zhang, Metall. Mater. Trans. A 36 (2005) 1681–1688.
[13] M.-X. Zhang, P.M. Kelly, Scr. Mater. 48 (2003) 647–652, doi:10.1016/S1359-6462(02)00555-9.
[14] C.R. Hutchinson, J.-F. Nie, S. Gorsse, Metall. Mater. Trans. A 36 (2005) 2093–2105.
[15] J.D. Robson, N. Stanford, M.R. Barnett, Metall. Mater. Trans. A. 44 (2013) 2984–2995, doi:10.1007/s11661-012-1466-0.
[16] B. Li, X.Y. Zhang, Scr. Mater. 125 (2016) 73–79, doi:10.1016/j.scriptamat.2016.07.004.
[17] M. Liao, B. Li, M.F. Horstemeyer, Comput. Mater. Sci. 79 (2013) 534–539, doi:10.1016/j.commatsci.2013.07.016.
[18] M. Liao, B. Li, M.F. Horstemeyer, Metall. Mater. Trans. A 45 (2014) 3661–3669, doi:10.1007/s11661-014-2284-3.
[19] Y.Z. Lü, Q.D. Wang, W.J. Ding, X.Q. Zeng, Y.P. Zhu, Mater. Lett. 44 (2000) 265–268.
[20] S.A. Salman, R. Ichino, M. Okido, Int. J. Corros. (2010) (2010) 1–7, doi:10.1155/2010/412129.
[21] M.-C. Zhao, M. Liu, G. Song, A. Atrens, Corros. Sci. 50 (2008) 1939–1953, doi:10.1016/j.corsci.2008.04.010.
[22] G. Han, Z. Han, A.A. Luo, A.K. Sachdev, B. Liu, Scr. Mater. 68 (2013) 691–694, doi:10.1016/j.scriptamat.2013.01.018.
[23] Z. Han, G. Han, A.A. Luo, B. Liu, Comput. Mater. Sci. 101 (2015) 248–254, doi:10.1016/j.commatsci.2015.01.038.
[24] G. Han, Z. Han, A.A. Luo, B. Liu, Metall. Mater. Trans. A 46 (2014) 948–962, doi:10.1007/s11661-014-2674-6.
[25] W. Xiao, X. Zhang, W.T. Geng, G. Lu, Mater. Sci. Eng. A 586 (2013) 245–252, doi:10.1016/j.msea.2013.07.093.
[26] M.S. Daw, M.I. Baskes, Phys. Rev. Lett. 50 (1983) 1285–1288, doi:10.1103/PhysRevLett.50.1285.
[27] M.S. Daw, M.I. Baskes, Phys. Rev. B 29 (1984) 6443.
[28] X.-Y. Liu, P.P. Ohotnicky, J.B. Adams, C.L. Rohrer, R.W. Hyland, Surf. Sci. 373 (1997) 357–370.
[29] B. Li, E. Ma, Philos. Mag. 89 (2009) 1223–1235, doi:10.1080/14786430902936707.
[30] B. Li, E. Ma, Acta Mater 57 (2009) 1734–1743, doi:10.1016/j.actamat.2008.12.016.
[31] B. Li, Q.W. Zhang, S.N. Mathaudhu, Scr. Mater. 134 (2017) 37–41, doi:10.1016/j.scriptamat.2017.02.040.
[32] Z. Wu, M.F. Francis, W.A. Curtin, Model. Simul. Mater. Sci. Eng. 23 (2015) 015004, doi:10.1088/0965-0393/23/1/015004.
[33] M.I. Baskes, Phys. Rev. B 46 (1992) 2727–2742, doi:10.1103/PhysRevB.46.2727.
[34] A. Stukowski, Model. Simul. Mater. Sci. Eng. 18 (2010) 015012.
[35] F. Wang, B. Li, in: D. Orlov, V. Joshi, K.N. Solanki, N.R. Neelameggham (Eds.), *Magnes Technol* 2018 (2018) 55–62.
[36] J.-M. Zhang, F. Ma, K.-W. Xu, Surf. Interface Anal. 35 (2003) 662–666, doi:10.1002/sia.1587.
[37] H. Ning, Z. Zhou, Z. Zhang, W. Zhou, G. Li, J. Guo, Appl. Surf. Sci. 396 (2017) 851–856, doi:10.1016/j.apsusc.2016.11.041.
[38] G. Han, Z. Han, A.L. Alan, K.S. Anil, B. Liu, Acta Metall. Sin. 49 (2013) 277, doi:10.3724/SP.J.1037.2012.00531.
[39] M. Li, Z. Ruijie, A. John, in: Proceedings of the Magnesium Technology 2010 Symposium held at the TMS 2010 Annual Meeting Exhibition, Minerals, Metals and Materials Society, 2010, pp. 623–627.
[40] Y. Minonishi, S. Ishioka, M. Koiwa, S. Mobozumi, Phys. Status Solidi A 71 (1982) 253–258, doi:10.1002/pssa.2210710130.